

advances.sciencemag.org/cgi/content/full/6/21/eaaz2059/DC1

Supplementary Materials for

A micropeptide encoded by lncRNA MIR155HG suppresses autoimmune inflammation via modulating antigen presentation

Liman Niu, Fangzhou Lou, Yang Sun, Libo Sun, Xiaojie Cai, Zhaoyuan Liu, Hong Zhou, Hong Wang, Zhikai Wang, Jing Bai, Qianqian Yin, Junxun Zhang, Linjiao Chen, Danhong Peng, Zhenyao Xu, Yuanyuan Gao, Sibe Tang, Li Fan, Honglin Wang*

*Corresponding author. Email: honglin.wang@sjtu.edu.cn

Published 20 May 2020, *Sci. Adv.* **6**, eaaz2059 (2020)

DOI: [10.1126/sciadv.aaz2059](https://doi.org/10.1126/sciadv.aaz2059)

The PDF file includes:

Figs. S1 to S5
Table S1

Other Supplementary Material for this manuscript includes the following:

(available at advances.sciencemag.org/cgi/content/full/6/21/eaaz2059/DC1)

Data files S1 and S2

Fig. S1

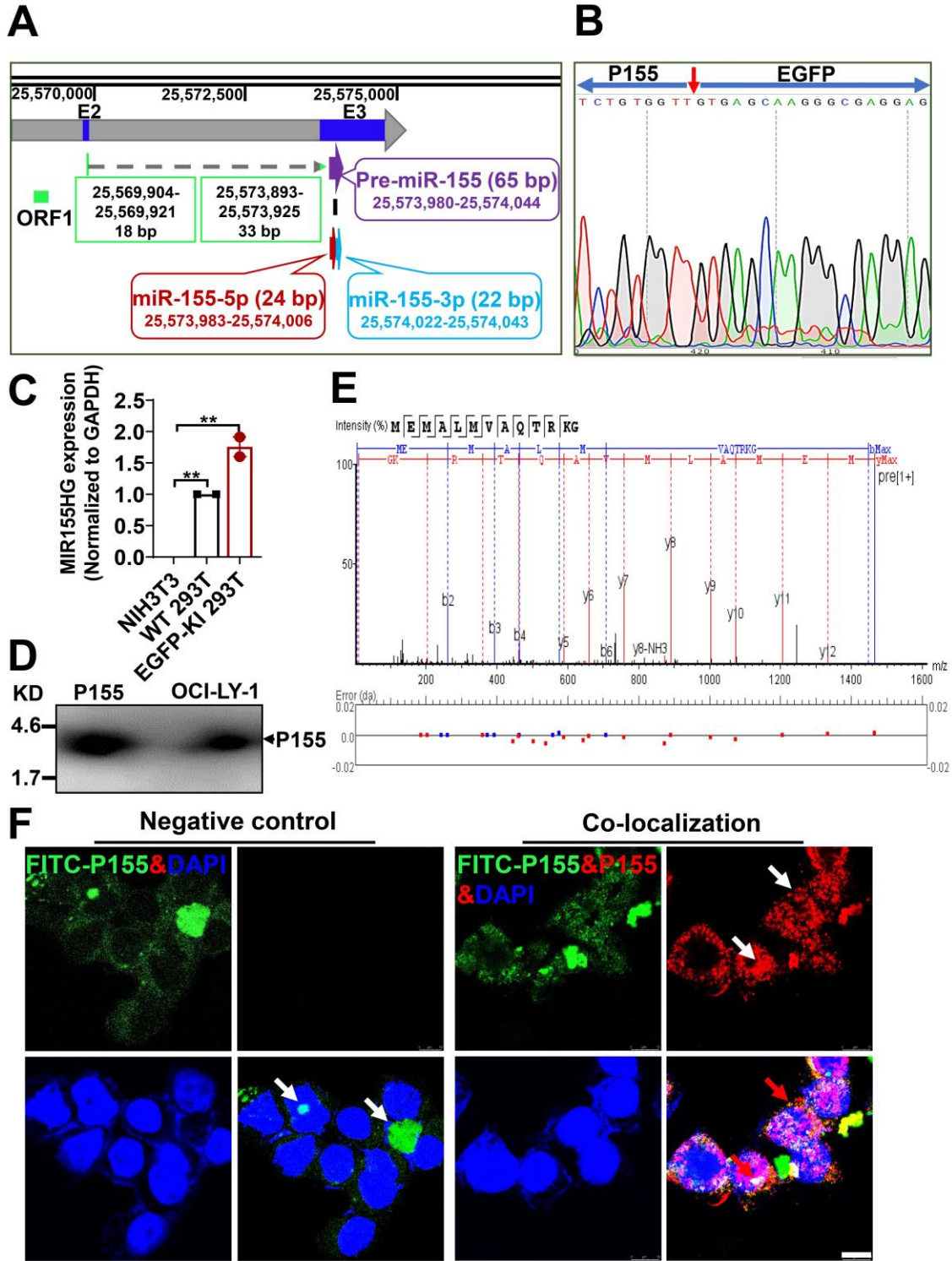
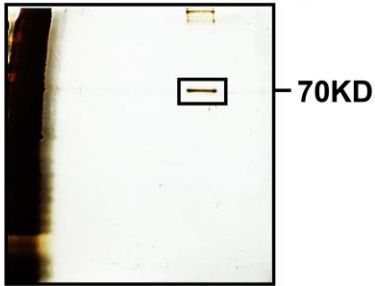


Figure S1. P155 endogenously-expressed in different kinds of cells. (A) Schematic representation of the ORF1 and Pre-miR-155 location in human *MIR155HG*. P155 is translated by ORF1 (marked with green); Pre-miR-155 is located at 55 bp after the stop codon of P155 (marked with purple); miR-155-5p (marked with red) and miR-155-3p (marked with bluish) were located within Pre-miR-155. (B) First-generation sequencing results of the engineered 293T cells. The red arrowhead indicates the interface between P155 and EGFP (without its own ATG). (C) qPCR data for *MIR155HG* expression in both NIH3T3, WT 293T and EGFP-KI 293T cells. Murine NIH3T3 cells served as a negative control. (D) Immunoblotting detection of endogenously-expressed P155 in OCI-LY-1 cells with P155-specific antibody pre-enrichment. Chemically-synthesized P155 served as a positive control, the target band is indicated by the black arrow. (E) LC-MS verification of the P155 endogenous expression in human moDCs with P155-specific antibody pre-enrichment. (F) Confocal microscopic images of the co-localization of endogenous and exogenous P155 in 293T cells. Nuclei were stained with DAPI (blue). FITC-P155 treated 293T cells without P155 primary antibody incubation served as a negative control. White arrowheads in negative control indicate the location of FITC-P155; white arrowhead in co-localization group indicates the location of endogenous P155 (red in nuclei and cytoplasm); the red arrowhead represents the co-localization of endogenous P155 and exogenous P155 (white in nuclei and yellow in cytoplasm). Scale bar represents 10 μm . $**P < 0.01$, one-way ANOVA (mean \pm SEM).

Fig. S2

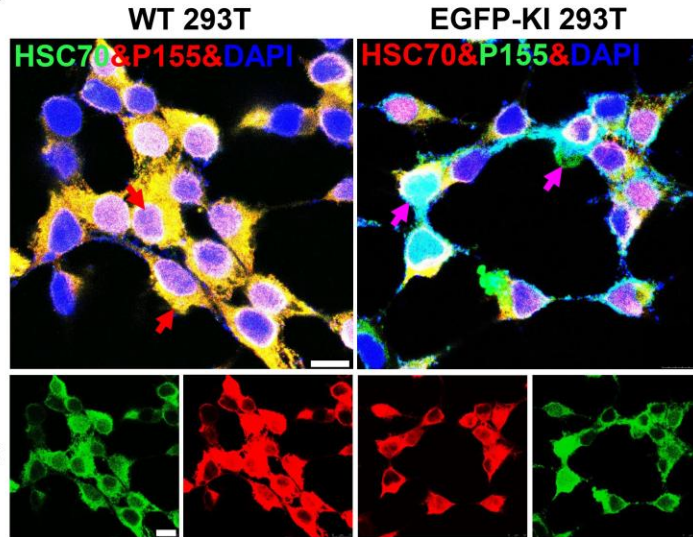
A

moDCs silver staining

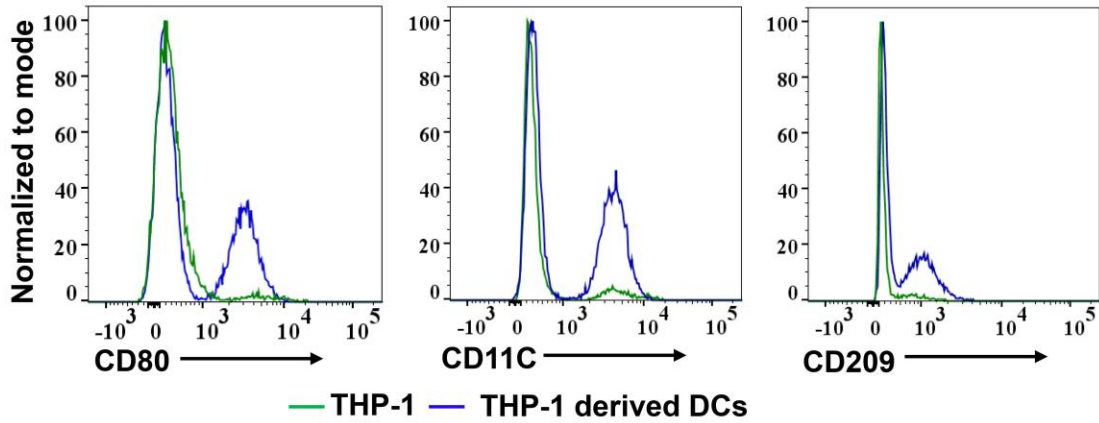


Input	+	-	-	-	-	Biotin
	-	+	-	-	-	Biotin-Scr
	-	-	+	-	-	Free-Scr
	-	-	-	+	+	Biotin-P155
	-	-	-	-	+	Free-P155
	+	+	+	+	+	R848

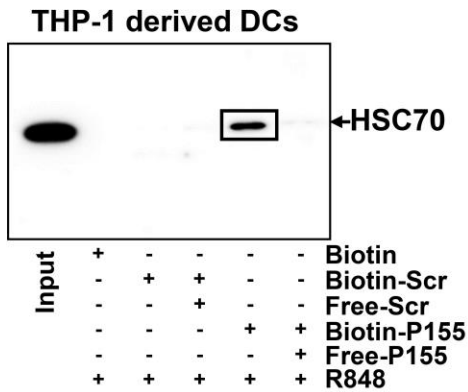
B



C



D



E

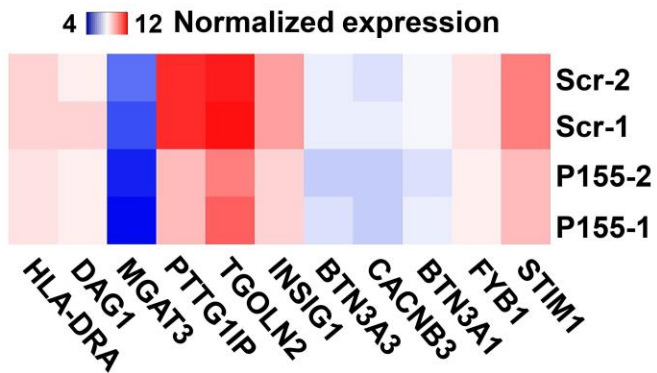


Figure S2. P155 combines with a ~ 73KD protein in human DCs and regulates the function of HSC70 as an antigen transporter. (A) The full gel picture of silver staining for P155 interactive protein in the immunoprecipitants pulled-down by streptavidin–agarose from R848 (1 µg/ml) and biotin-Scr/P155 (25 µM) pre-treated human moDCs. The black box represents the target protein. (B) Confocal microscopic images of the co-localization of P155 and HSC70 in WT 293T and EGFP-KI 293T cells. Nuclei were stained with DAPI (blue). Red/Pink arrowheads indicate the co-localization of P155 and HSC70 in WT 293T cells (white in nuclei and yellow in cytoplasm) and in EGFP-KI 293T cells (bluish in nuclei and green in cytoplasm). (C) Representative flow cytometry charts of CD80, CD11C and CD209 expression in THP-1-derived DCs. (D) Immunoblotting verification of the interaction between P155 and HSC70 in THP-1-derived DCs. The black box indicates the specific band. (E) Heat map of selected genes based on RNA-seq data from R848 (1 µg/ml) and Scr/P155 (25 µM) pre-treated THP-1-derived DCs ($p < 0.05$, $\text{Log}_2\text{FC} < -1$, $n = 2$). Color key represents the normalized expression of genes. Scale bars represent 10 µm.

Fig. S3

A

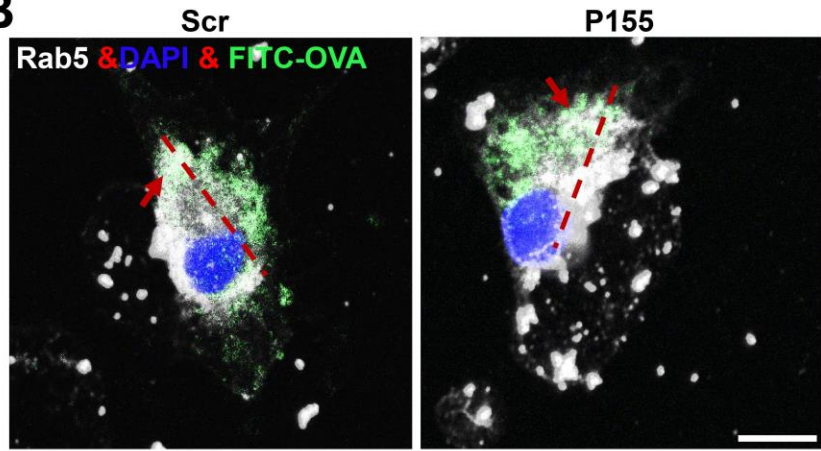
Homo HSC70 VS Mus HSC70:Per.Ident:99.85%

```

mskgrpavgidlgttyscvgvfghgkveiandqgnrttpsyvaftdterligdaaknqvampntntvfdakrligrffddavvqsd
*****
mkhwpfmvndagrpkvqveykgetksfypeevssmvltkmkeiaeylgktvnavvtvpayfndsqrqatkdagtiaglNvlRi
*****
ineptaaaiaygldkkvgaernvlifdlgggtfdvsiiltiedgifevkstagdthlggedfndrmvnhfiaefkrkhkhdisenkr
*****
avrrlrtacerakrtlssstqasieidslyegidfytsitrarfeelnadlfrgtldpvekalrdakldksqihdivlvggstr ip
*****
kiqklldqffngkelnksinpdeavaygaavqaaaisgdksenvqdlldvtpslslietaggvmtvlkrnttipktqtftt
*****
ysdnqpgvliqvyegeramtkdnnlkgfeltgippaprgvpqievtfdidangiInvsavdkstgkenkititndkgrlskedie
*****
RmvqeaekykaedekqrdkvssknslesyafnmkatvedeklqgkinedkqkiIdkcneiInwldknqtaekee fehqqkelekv
*****
cnpitklyqsaggmpggmpggfpgggappsggassgptieevd
*****

```

B



C

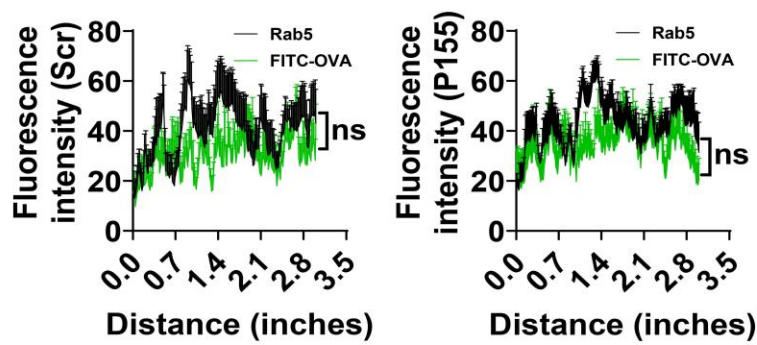


Figure S3. Human and mouse HSC70 shares highly homology and the endosome is not essential for P155 regulated antigen transport. (A) Alignment of full-length HSC70 amino acid sequences from human (blue) and mouse (gray). Conserved amino acids are indicated by asterisks, and the non-conserved amino acid sequences are marked in red. (B) Confocal microscopic images of mouse BMDCs treated with FITC-OVA, with the cells co-stained with Rab5 (white) and nuclei stained with DAPI (blue). The red arrowheads indicate the co-localization of FITC-OVA and Rab5 (bright green). The red dotted line represents the position indicator for the fluorescence co-localization analysis. (C) Fluorescence intensity analysis of co-localization of FITC-OVA and Rab5 in mouse BMDCs treated with Scr or P155 (n = 6). Image J software was used to analyze the fluorescence intensity of co-localization. The red dotted indicator line of statistical analysis centers on the co-colocation of FITC-OVA and Rab5. Scale bar represents 10 μ m. ns, not significant, one-way ANOVA (mean \pm SEM).

Fig. S4

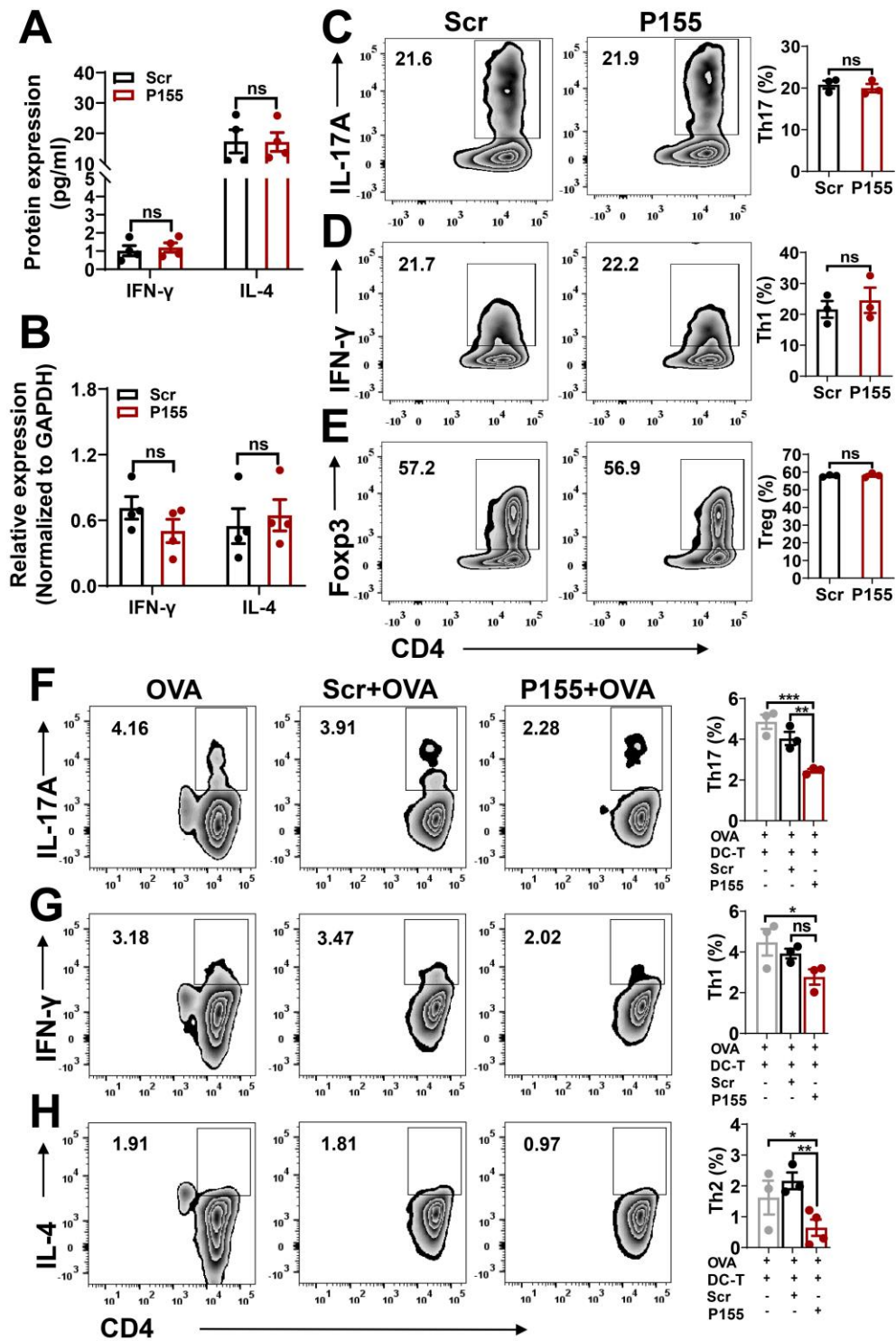


Figure S4. P155 does not directly monitor T cell differentiation, but modulates antigen presentation to skew T cell polarization statuses. (A) ELISA quantification of IFN- γ and IL-4 protein expression in supernatants of Scr or P155 treated IMQ-induced mouse ear homogenates (n = 4). (B) qPCR data for IFN- γ and IL-4 mRNA expression in Scr or P155 treated IMQ-induced mouse ear. (C-E) Representative flow cytometry charts (left) and quantification (right) of Th17 (C), Th1 (D) and Treg (E) cells percentages in Scr or P155 treated Naïve CD4⁺ splenic T cells under respective differentiation conditions (n = 3). (F-H) Representative flow cytometry charts (left) and quantification (right, indicated by CD44⁺CD4⁺Violet⁻ cell percentages) of Th17 cells (F), Th1 cells (G) and Th2 cells (H) percentages in OT-II CD4⁺ T cells co-cultured with OVA-loaded BMDCs in the presence of P155 or Scr treatment (n = 3-4). DC-T: BMDCs co-cultured with OT-II CD4⁺ T cells. Data (C-E) represents of three independent experiments. ns, not significant; * $P < 0.05$; ** $P < 0.01$; *** $P < 0.001$, one-way ANOVA (mean \pm SEM).

Fig. S5

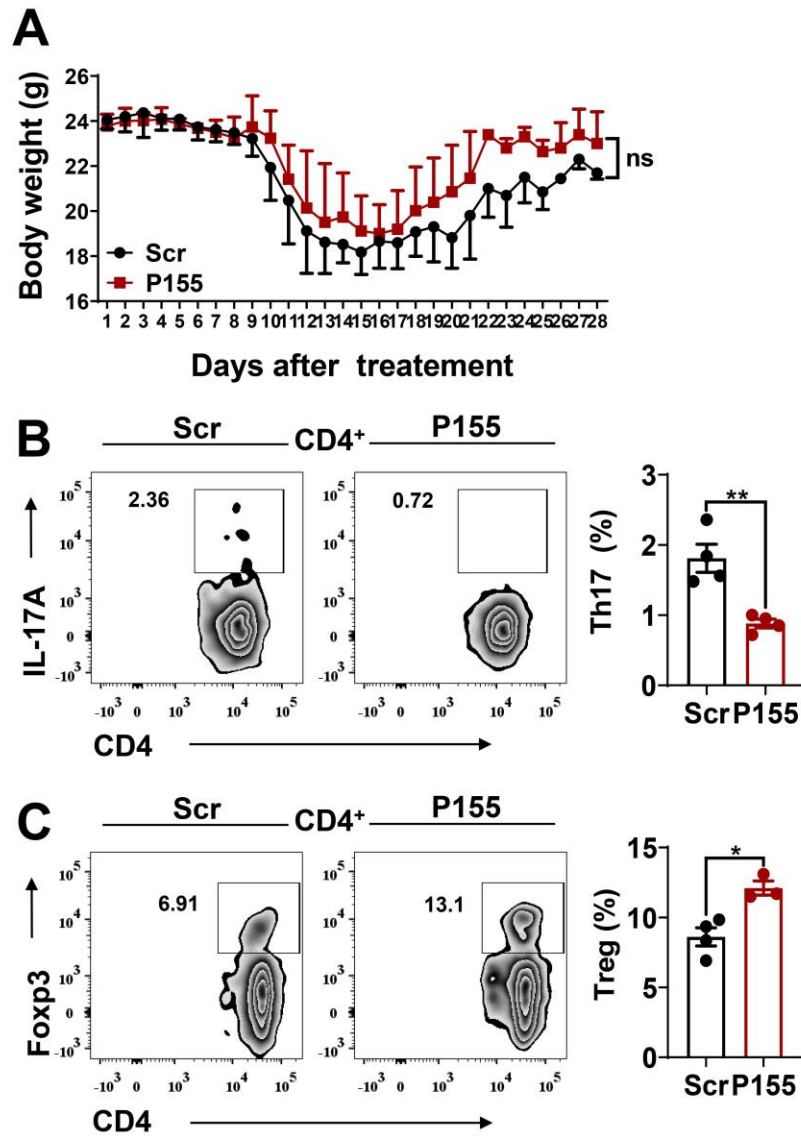


Figure S5. P155 exhibits no toxicity and affects splenocytes expression in EAE mouse model. (A) Calculation of body weight in Scr or P155 treated EAE mice (n = 5). (B and C) Representative flow cytometry charts and quantification of Th17 cells (B) and Treg cells (C) gated on CD4⁺ T cells in Scr or P155 treated EAE mouse spleens on Day 15 post-immunization (n = 3-4). Data are representative of three independent experiments. ns, not significant; **P* < 0.05; ***P* < 0.01, one-way ANOVA (mean ± SEM).

Table. S1

AUG initiated sORFs		
Label	Protein Sequence	Length (nt)/aa
ORF1	MEMALMVAQTRKGKSVV	54/17
ORF4	MPHPLSAEGLL	36/11
ORF2	MLLMLVIGVFASN	45/14
ORF10	MMPVTSIHMEQIAAVGG	54/17
ORF5	MTKKHESPCWINLDFRLYHFSIC	72/23
ORF11	MFNLKLSFESKVI	42/13
ORF6	MQTFSFKCQAHVCFYH	51/16
ORF3	MSSPCLFLSLTENIFMSFLIAGFGLFIIMFINTFDSTVRNVG	129/42
ORF12	MFVFIINRKYIHVILNCRFWLVHYNVHKHL	93/30
ORF7	MDCLATFFKRFRNWFYPPGNDFLFRQLQFKINTFI	108/35
ORF8	MKLNFFNEIFLTVSRVNNI	60/19
ORF9	MGIILYKVVVRLR	42/13
non-AUG initiated sORFs		
ORF20	MALQITCLHFKNNLPETLPVTALPPNGDGSNGGTNQEGEIC GLNSLCLIL	156/51
ORF11	MSAFQEQPTRDLTCHLGSPTQWRWL	78/25
ORF1	MSPWLSHPMEMALMVAQTRKGKSVV	78/25
ORF12	MWFKFFMPHPLSAEGLL	54/17
ORF21	MKACCRLYAVNANRDRGFCLQLTPTY	81/26
ORF2	MLLMLVIGVFASN	45/14
ORF13	MPPTDSYILALTVYDACV	57/18
ORF22	MMPVTSIHMEQIAAVGG	54/17
ORF3	MLLAFTWNKLLPWEDDKEA	60/19
ORF14	MTKKHESPCWINLDFRLYHFSIC	72/23
ORF4	MLDKLRLQALSFFNLLIIWSLGCSTLN	87/28
ORF23	MVTGMFNLKLSFESKVI	54/17
ORF5	MKVRLFKRFISSILNANIFI	63/20
ORF15	MQTFSFKCQAHVCFYH	51/16
ORF6	MSSPCLFLSLTENIFMSFLIAGFGLFIIMFINTFDSTVRNVG	129/42
ORF24	MFVFIINRKYIHVILNCRFWLVHYNVHKHL	93/30
ORF16	MIQLLEMWAKHKFL	45/14
ORF17	MDCLATFFKRFRNWFYPPGNDFLFRQLQFKINTFI	108/35
ORF7	MTLKGKLGYEAEFF	48/15
ORF18	MKLNFFNEIFLTVSRVNNI	60/19
ORF8	MTANEIFFPYKIKRFNQKISYLK	72/23
ORF25	MCEQRIYLSKPVSSSIWG	63/20
ORF19	MGIILYKVVVRLR	42/13
ORF9	MFLPPYGDNTLQGCCEA	54/17
ORF10	MICRIFKVVISMQFF	48/15
ORF26	MDFYAVFLNNHHLQICNQT	60/19

Table S1. A datasheet of all the sense ORFs (AUG and non-AUG initiated) of MIR-155HG identified by ORFfinder.